INTERNATIONAL JOURNAL FOR NUMERICAL METHODS IN ENGINEERING

*Int. J. Numer. Meth. Engng* 2006; **00**:1–16 *Prepared using* nmeauth.cls *[Version: 2002/09/18 v2.02]*

# A Family of Large-Stencil Discrete Laplacian Approximations in Three Dimensions

Randall C. O'Reilly*and Jeffrey M. Beck

*University of Colorado Boulder, 345 UCB, Boulder, CO 80309*

SUMMARY

A family of discrete approximations to the Laplacian operator with increasingly large stencil sizes for explicit (forward) Euler integration is derived and analyzed. This family includes a 19-point stencil described earlier by Barkley and colleagues, and a new 27-point stencil. This 27-point stencil, which includes all 26 adjacent neighbors in a face-centered regular cubic tiling of three-dimensional space (faces, edges, and corners), has a maximum stable time step parameter $\Delta t_{max}$ of .5 for the first-order diffusion equation, and 1 for the second-order wave equation. In contrast, the standard 7-point stencil has a first-order $\Delta t_{max} = .166\overline{6}$ and the 19-point stencil $\Delta t_{max} = .375$. Because these neighborhood calculations are easily vectorized on modern processors, the larger stencils do not incur substantially greater computational cost, resulting in significant overall speedup from the larger step size (e.g., 2.58 times faster for the 27-point stencil relative to the standard 7-point in our benchmark). The larger neighborhood stencils also exhibit significantly greater rotational symmetry than the standard approximation. In a numerical test with a spherical perturbation propagating via the wave equation, the 7-point stencil exhibited 17% error levels, whereas the 19-point stencil error was only 1%. Thus, these new approximations afford significant advantages over the standard one. 

KEY WORDS: Discrete element method Eulerian, Elliptic partial differential equations, Explicit time integration

*Correspondence to: University of Colorado Boulder, 345 UCB, Boulder, CO 80309, Randy.OReilly@colorado.edu.

*Received October 14, 2006*

## 1. Introduction

The Laplacian operator $\nabla^2$ is the critical computation in several important equations, including the wave and diffusion equations, which occur widely across every branch of physics. To numerically solve these equations in three dimensions on a computer, a three-dimensional discrete approximation is required. The standard approximation for explicit (forward) Euler integration with a regular face-centered cubic tiling of space uses a 7-point stencil involving the central point and its 6 nearest neighbors along adjacent faces. A 19-point stencil that includes the 6 adjacent faces and the 12 next-nearest edge neighbors was described by Barkley and colleagues [1], which has two key advantages: a maximum stable time step that is 2.25 times larger than the 7-point case, and a significant reduction of grid anisotropies (rotational asymmetry) because the leading contributions to error are invariant under rotations. Here, we describe an even larger 27-point stencil that includes the 8 corner neighbors in addition to faces and edges, and has an even larger maximum stable time step ($1.33\overline{3}$ times larger than the 19-point, and 3 times larger than the 7-point).

## 2. Derivation of the 19-point Stencil

The Laplacian is the divergence of the gradient:

$$\nabla^2 \equiv \vec{\nabla} \cdot \vec{\nabla} \equiv \frac{\partial^2}{\partial x^2} + \frac{\partial^2}{\partial y^2} + \frac{\partial^2}{\partial z^2}, \tag{1}$$

which appears in the standard second-order wave equation:

$$\frac{\partial^2 \varphi}{\partial t^2} = c^2 \nabla^2 \varphi, \tag{2}$$

where $0 < c < 1$ controls the speed of wave propagation.

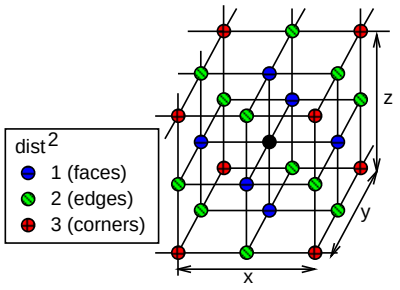


Figure 1. Face-centered cubic tiling of space, showing centers of cells as nodes, with all 26 neighbors of a given cell shown. The standard discrete approximation uses only the 6 face neighbors. Other approximations here enable all 26 to be used.

For a discrete one-dimensional field $\varphi_i$ with grid spacing $h$, the second spatial derivatives can be approximated by taking the difference of two first order difference equations:

$$\begin{aligned} \frac{\partial \varphi}{\partial x} \approx D^- \varphi_i &= \frac{1}{h}(\varphi_i - \varphi_{i-1}) \\ \approx D^+ \varphi_i &= \frac{1}{h}(\varphi_{i+1} - \varphi_i) \\ \frac{\partial^2 \varphi}{\partial x^2} \approx \frac{1}{h}(D^+ \varphi_i - D^- \varphi_i) &= \frac{1}{h^2}(\varphi_{i+1} + \varphi_{i-1} - 2\varphi_i). \end{aligned} \tag{3}$$

In a discretized three-dimensional space using a face-centered cubic tiling (Figure 1, grid spacing $h$), the standard approximation is to simply apply the one-dimensional discretization to each of the three axes, using the 6 face neighbors:

$$\begin{aligned} \nabla_f^2 \varphi_i &= \frac{1}{h^2}\left(\varphi_{(1,0,0)} + \varphi_{(-1,0,0)} + \varphi_{(0,1,0)} + \varphi_{(0,-1,0)} + \varphi_{(0,0,1)} + \varphi_{(0,0,-1)} - 6\varphi_i\right) \\ &= \frac{1}{h^2} \sum_{j \in \mathcal{N}_f} \varphi_j - 6\varphi_i \\ &= \frac{1}{h^2} \sum_{j \in \mathcal{N}_f} (\varphi_j - \varphi_i), \end{aligned} \tag{4}$$

where $\nabla_f^2$ denotes the face-based approximation and $\varphi_{(x,y,z)}$ indicates the neighbor at the given $(x, y, z)$ offset from the point being computed ($\varphi_i$). This set of 6 neighbors is denoted $\mathcal{N}_f$ (faces). The final form shows that each neighbor contributes the difference between its value and the central

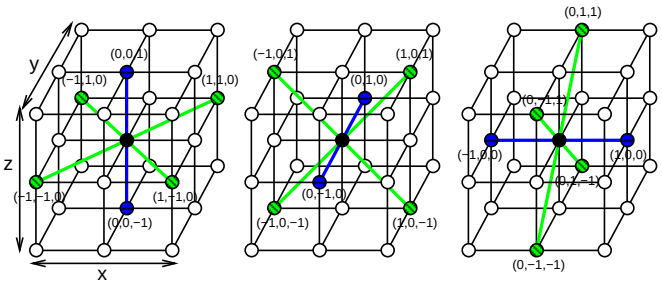


Figure 2. Three sets of orthogonal axes involving faces and edges, which includes all 18 of these neighbors, with no overlap across sets. A more stable 19-point stencil approximation to the Laplacian can be constructed by averaging across these sets.

value to the overall sum.

A problem with this standard approximation is that, in the wave equation, many of the neighboring points in space are not directly affected by a disturbance propagating along a non-cartesian axis, because a given cell is only influenced by this small subset of neighbors. This introduces preferred directions of wave propagation (anisotropy), and also leads to numerical instability.

One strategy for including a larger set of neighbors in the Laplacian calculation is to construct three new orthogonal basis sets from the face and edge points, as shown in Figure 2. Each set of neighbors has no overlap with the others, and together they include all of the face and edge points. Therefore, we can include all of the face and edge neighbors by averaging across these three basis cases:

$$\begin{aligned} \nabla^2_{fe}\varphi_i &= \frac{1}{3h^2}\left(\sum_{j\in\mathcal{N}_f}(\varphi_j-\varphi_i)+\frac{1}{2}\sum_{j\in\mathcal{N}_e}(\varphi_j-\varphi_i)\right) \\ &= \frac{1}{3h^2}\left(\sum_{j\in\mathcal{N}_f}\varphi_j+\frac{1}{2}\sum_{j\in\mathcal{N}_e}\varphi_j-12\varphi_i\right) \\ &= \frac{1}{6h^2}\left(2\sum_{j\in\mathcal{N}_f}\varphi_j+\sum_{j\in\mathcal{N}_e}\varphi_j-24\varphi_i\right) \end{aligned} \tag{5}$$

where the $\frac{1}{3}$ factor comes from the averaging of the three basis sets, and the $\frac{1}{2}$ factor for the edges reflects a normalization by the distance to the edge neighbors. The last form shown above is equivalent

to the 19-point stencil (18 neighbors = 6 faces + 12 edges) derived by Barkley and colleagues [1].

## 3. Stability Analysis of the 19-point Stencil

We reproduce here the stability analysis (in slightly more detail) of the 19-point stencil as performed by Barkley and colleagues [1], which we will extend to the 27-point case later. The overall strategy is to perform an eigenvalue analysis, where stability requires that the largest eigenvalue have a magnitude of less than 1.

First, the first-order diffusion equation is considered, because it is simpler to analyze than the second-order wave equation (which we analyze in a subsequent section; the maximum stable time step for the second order equation is twice that of this first-order one):

$$\frac{\partial u}{\partial t} = \nabla^2 u. \tag{6}$$

Using the 19-point faces + edges approximation and explicit-Euler time stepping, this is:

$$\begin{aligned} u_i^{n+1} &= u_i^n + \Delta t \nabla_{fe}^2 \\ &= u_i^n + \Delta t \frac{1}{3h^2} \left( \sum_{j \in \mathcal{N}_f} u_j^n + \frac{1}{2} \sum_{j \in \mathcal{N}_e} u_j^n - 12 u_i^n \right). \end{aligned} \tag{7}$$

This can be expressed as a linear equation:

$$u_{ijk}^{n+1} = \mathbf{A} u_{ijk}^n, \tag{8}$$

where the matrix $\mathbf{A}$ contains the neighborhood weighting factors:

$$\mathbf{A} = 1 + \nabla_{fe}^2. \tag{9}$$

This linear equation can be expressed in terms of eigenvalues $\lambda$ operating on a rotated eigenfunction representation of the state values, $\psi$:

$$\mathbf{A} \psi_{ijk} = \lambda \psi_{ijk}. \tag{10}$$

The system is stable as long as all eigenvalues $\lambda$ of the matrix $\mathbf{A}$ have a magnitude 1 or less. The eigenfunctions of $\mathbf{A}$ are discrete forms of the eigenfunctions of the Laplacian:

$$\psi_{ijk} = cos(l_x i)cos(l_y j)cos(l_z k), \tag{11}$$

where $l_x, l_y, l_z$ are wavenumbers, and sine can replace any of the cosines as well.

To determine these eigenvalues, we write out all the terms of $\mathbf{A}$ and $\lambda$, and then derive a condensed expression. First, we set:

$$\epsilon = \frac{\Delta t}{3h^2} \tag{12}$$

and write $\mathbf{A}$ for each of the $x, z$ planes along the different slices of $y = \{-1, 0, 1\}$:

$$\begin{aligned}
\mathbf{A}_{y=-1} &= \begin{pmatrix} 0 & \frac{\epsilon}{2} & 0 \\ \frac{\epsilon}{2} & \epsilon & \frac{\epsilon}{2} \\ 0 & \frac{\epsilon}{2} & 0 \end{pmatrix} \\
\mathbf{A}_{y=0} &= \begin{pmatrix} \frac{\epsilon}{2} & \epsilon & \frac{\epsilon}{2} \\ \epsilon & 1-12\epsilon & \epsilon \\ \frac{\epsilon}{2} & \epsilon & \frac{\epsilon}{2} \end{pmatrix} \\
\mathbf{A}_{y=+1} &= \begin{pmatrix} 0 & \frac{\epsilon}{2} & 0 \\ \frac{\epsilon}{2} & \epsilon & \frac{\epsilon}{2} \\ 0 & \frac{\epsilon}{2} & 0 \end{pmatrix}.
\end{aligned} \tag{13}$$

Substituting in the Laplacian eigenfunctions (11), this is:

$$\begin{aligned}
\lambda_{y=-1} &= \begin{pmatrix} 0 & \frac{\epsilon}{2}\cos(-l_y)\cos(l_z) & 0 \\ \frac{\epsilon}{2}\cos(-l_x)\cos(-l_y) & \epsilon\cos(-l_y) & \frac{\epsilon}{2}\cos(l_x)\cos(-l_y) \\ 0 & \frac{\epsilon}{2}\cos(-l_y)\cos(-l_z) & 0 \end{pmatrix} \\
\lambda_{y=0} &= \begin{pmatrix} \frac{\epsilon}{2}\cos(-l_x)\cos(l_z) & \epsilon\cos(l_z) & \frac{\epsilon}{2}\cos(l_x)\cos(l_z) \\ \epsilon\cos(-l_x) & 1-12\epsilon & \epsilon\cos(l_x) \\ \frac{\epsilon}{2}\cos(-l_x)\cos(-l_z) & \epsilon\cos(-l_z) & \frac{\epsilon}{2}\cos(l_x)\cos(-l_z) \end{pmatrix} \\
\lambda_{y=+1} &= \begin{pmatrix} 0 & \frac{\epsilon}{2}\cos(l_y)\cos(l_z) & 0 \\ \frac{\epsilon}{2}\cos(-l_x)\cos(l_y) & \epsilon\cos(l_y) & \frac{\epsilon}{2}\cos(l_x)\cos(l_y) \\ 0 & \frac{\epsilon}{2}\cos(l_y)\cos(-l_z) & 0 \end{pmatrix}.
\end{aligned} \tag{14}$$

Because cosine is symmetric about zero ($\cos(-l_x) = \cos(l_x)$), we can group like terms and get:

$$\begin{aligned}
\lambda &= 1 + 2\epsilon \quad [\cos(l_x) + \cos(l_y) + \cos(l_z) + \\
&\qquad \cos(l_x)\cos(l_y) + \cos(l_y)\cos(l_z) + \cos(l_x)\cos(l_z) - 6]\,.
\end{aligned} \tag{15}$$

The term inside the brackets has its largest magnitude at a value of -8, which occurs when any two of the wavenumbers are $\pi$ and the third is 0. Thus, the overall largest magnitude eigenvalue is:

$$\lambda_{max} = 1 - \frac{16\Delta t}{3h^2}, \tag{16}$$

which means that the limiting $\Delta t$ value required to keep $|\lambda_{max}| < 1$ is:

$$\Delta t_{max} = \frac{3}{8}h^2 = .375h^2. \tag{17}$$

Compare this with the corresponding value for the standard 7-point face-only stencil:

$$\Delta t_{max} = \frac{1}{6}h^2 = .166\overline{6}h^2. \tag{18}$$

Thus, the 19-point stencil can be run 2.25 times faster than the 7-point case.

Furthermore, the error in this approximation is given by [1]:

$$E = \frac{h^2}{12}(\nabla^2)^2 u|_{ijk} + O(h^4). \tag{19}$$

Because the leading term is the squared Laplacian, which is rotationally symmetric, this approximation exhibits much greater rotational symmetry (i.e., propagation along non-cartesian gridlines) than the standard 7-point approximation, which does not have a rotationally symmetric leading error term.

## 4. Extension to the 27-point Stencil

Although better than the 7-point stencil, the 19-point face + edge approximation still leaves out 8 of the neighbors: the corners. These are tricky because they do not form an orthogonal basis. Nevertheless, we can construct a stencil that includes them (a 27-point stencil) by noting that in the 19-point case, each neighbor contributes according to the following equation:

$$\frac{1}{||j-i||}(\varphi_j - \varphi_i), \tag{20}$$

where $||j-i||$ is the squared distance between the neighbor point $j$ and the central point $i$ (i.e., 1 for faces, 2 for edges, and 3 for corners). Furthermore, the sum is normalized by:

$$\frac{6}{N_{points}h^2}. \tag{21}$$

The 6 in the numerator comes from the fact that the canonical face-based Laplacian consists of 6 neighbor points located at the ends of the 3 rays that define the three second derivatives $\left(\frac{\partial^2\varphi}{\partial x^2} + \frac{\partial^2\varphi}{\partial y^2} + \frac{\partial^2\varphi}{\partial z^2}\right)$, which is then divided by the total number of points included in the sum ($N_{points}$; note that this the number of neighbors, excluding the central point).

These equations can be used to define a whole family of Laplacians involving various combinations of the faces, edges and corners, including faces only (7-point stencil; equation 4), faces + edges (19-

point stencil; equation 5), and faces + edges + corners (27-point stencil):

$$\begin{aligned}\nabla^2_{fec}\varphi_i &= \frac{3}{13h^2}\left(\sum_{j\in\mathcal{N}_f}(\varphi_j-\varphi_i)+\frac{1}{2}\sum_{j\in\mathcal{N}_e}(\varphi_j-\varphi_i)+\frac{1}{3}\sum_{j\in\mathcal{N}_c}(\varphi_j-\varphi_i)\right)\\ &= \frac{3}{13h^2}\left(\sum_{j\in\mathcal{N}_f}\varphi_j+\frac{1}{2}\sum_{j\in\mathcal{N}_e}\varphi_j+\frac{1}{3}\sum_{j\in\mathcal{N}_c}\varphi_j-\frac{44}{3}\varphi_i\right)\end{aligned} \tag{22}$$

(see the Appendix for another derivation based on including additional neighbors in the first order gradient computation that also yields equation 22).

### *4.1. Stability Analysis of the 27-point Stencil*

Applying the eigenvalue stability analysis from the 19-point case to this 27-point stencil, the $\lambda$ matrix just adds 8 new terms for the corners, each of the form: $\frac{\epsilon}{3}\cos(\pm l_x)\cos(\pm l_y)\cos(\pm l_z)$, where the $\epsilon$ factor is now:

$$\epsilon = \frac{3\Delta t}{13h^2}. \tag{23}$$

Because of the cosine symmetry, the resulting eigenvalue equation includes just one additional term for the 8 corner factors, and the subtraction value for the central point is different:

$$\begin{aligned}\lambda = 1+2\epsilon \quad & [\cos(l_x)+\cos(l_y)+\cos(l_z)+\\ & \cos(l_x)\cos(l_y)+\cos(l_y)\cos(l_z)+\cos(l_x)\cos(l_z)+\\ & \frac{4}{3}\cos(l_x)\cos(l_y)\cos(l_z)-\frac{22}{3}\Big].\end{aligned} \tag{24}$$

The term inside the brackets has its largest magnitude at a value of $-8.66\overline{6}$, which occurs when the wavenumbers for all dimensions are $\pi$, and when only one wavenumber is $\pi$ and the others are 0. Thus, the overall largest magnitude eigenvalue is:

$$\lambda_{max} = 1-\frac{52\Delta t}{13h^2}, \tag{25}$$

which means that the limiting $\Delta t$ value required to keep $|\lambda_{max}| < 1$ is:

$$\Delta t_{max} = \frac{13}{26} h^2 = .5h^2 \tag{26}$$

This is $1.33\overline{3}$ times larger than the $\Delta t_{max}$ for the 19-point case, and 3 times larger than for the 7-point case.

## 5. Second-Order Wave Equation

Now we extend the stability analysis to the second-order wave equation. Letting $u_i^n = \lambda^n$, we conclude that the discrete dynamical system is stable when

$$\lambda = 1 + 2\frac{\Delta t}{\Delta h^2}\gamma \tag{27}$$

is between -1 and 1 ($\gamma$ is short for the coefficients in the Laplacian as well as the cosine terms). Because $\gamma$ is always negative and bounded below by $\gamma_{min}$ only the lower bound need be considered. Thus stability is insured when

$$\Delta t \leq \frac{\Delta h^2}{\gamma_{min}}. \tag{28}$$

In the second-order wave equation, the update rule is now:

$$u_i^{n+1} - 2u_i^n + u_i^{n-1} = u_i^n 2\frac{\Delta t^2}{\Delta h^2}\gamma. \tag{29}$$

We once again let $u_i^n = \lambda^n$, so that

$$\lambda^2 - 2\lambda\left(1 + \frac{\Delta t^2}{\Delta h^2}\gamma\right) + 1 = 0 \tag{30}$$

defines the eignenvalues of the system. In this quadratic case, $|\lambda| \leq 1$ is insured when

$$-1 \leq 1 + \frac{\Delta t^2}{\Delta h^2}\gamma \leq 1. \tag{31}$$

Again $\gamma$ is negative and bounded below by $\gamma_{min}$ so that only the lower bound need be considered. Thus stability is insured when

$$\Delta t^2 \leq 2\frac{\Delta h^2}{\gamma_{min}}. \tag{32}$$

From this we can conclude that the maximum stable time step for the wave equation (second order) is related to that of the first-order diffusion (heat) equation as:

$$\Delta t_{wave} = \sqrt{2\Delta t_{heat}}. \tag{33}$$

This general property of any numerical algorithm which iteraties time using the standard forward Euler method implies that the maximum stable time step for the wave equation using the 27-point stencil is $1h^2$.

## 6. Computational Speed and Error Due to Rotational Asymmetry

There are two factors that determine the overall computational speed of these Laplacian approximations: the maximum stable time step (the larger the step, the fewer iterations required to solve the equations over a given amount of physical time), and the amount of computation per time step. It may seem that the increase in stable time step associated with the larger stencil approximations is more than offset by the larger number of neighbors that must be computed over at each time step. However, it is critical to appreciate that this neighborhood stencil computation is highly parallelizable on modern vectorizing processors, such that increasing the stencil size results in a relatively small increase in net computation time. Thus, the increase in stable time step dominates the overall computational cost. This is especially true when solving more complex equations involving the Laplacian as only one component (albeit the stability limiting one), where the overhead of other computations per time step is relatively large, and thus the larger time step results in even greater speedups.

As a simple benchmark for computational speed, we implemented the basic diffusion equation (6) using the different stencil sizes on a modern Pentium processor using the gcc compiler (4.0.2) under Linux. We first measured the differences in computational cost associated with the different stencil sizes, keeping the number of iterations constant (i.e., using the same time step for each). It took 2.13, 2.03, and 1.83 seconds respectively for the 27, 19, and 7 point stencils to compute 200 iterations over a 30x30x30 space, using a time step of .1. Thus, the increase of 20 additional neighbors for the 27-point stencil relative to the standard 7-point case requires only 16% additional computation time. This clearly demonstrates a significant degree of parallelization of this stencil computation. When we combine this per-time-step computational cost factor with the differences in maximum stable time step (.5, .375, and $.166\overline{6}$ for 27, 19, and 7-point stencils), the 27-point case is 2.58 times faster overall compared to the 7-point case, and the 19-point stencil is 2.03 times faster. This represents a significant computational savings, approaching the theoretical maximum speedups if the neighborhood calculation were perfectly parallel (3 and 2.25). Indeed, these theoretical maximums may be achievable on specialized parallel hardware, providing an even greater computational speedup.

The other principal advantage of the larger stencil size is its greater rotational symmetry, which results in more accurate simulation of perturbations that have spatial structure across multiple dimensions (this will not be evident in plane waves, for example). To explore the significance of rotational symmetry, we initialized the state with a spherically-symmetric non-normalized Gaussian perturbation (i.e., $e^{-\frac{||\vec{i}-\vec{\mu}||}{\sigma^2}}$) with the center point located in the center of a 50x50x50 space ($\vec{\mu} = (25, 25, 25)$). The width of the Gaussian $\sigma$ was set to 2. This perturbation should remain symmetric as it spreads via the standard wave equation (2). To measure the rotational asymmetry of this wave propagation, we sorted the state cells as a function of distance from the center of the initial Gaussian, and computed the mean and standard deviation of values at the same distance (Figure 3). With this

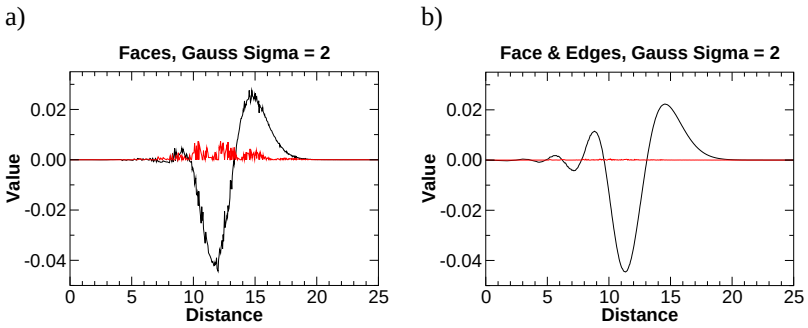


Figure 3. Contributions of rotational asymmetry to error in the standard 7-point stencil, compared with larger stencil-size approximations (using the standard wave equation). Plots show mean wave value (large amplitude wavy line) and average error (standard deviation, smaller amplitude line) for state cells as a function of distance from the center of an initial rotationally symmetric Gaussian ($\sigma = 2$, 30 time steps, $\Delta t = .2$ for all cases). **a)** $\nabla^2_f$ (7 point stencil), which exhibits significant error (nearly 17% of maximum wave magnitude), consistent with its greater anisotropy (rotational asymmetry). **b)** $\nabla^2_{fe}$ (19-point stencil) has much lower error (1% of maximum wave magnitude).

analysis, all points at different rotational angles from the center, including those along cartesian axes and not, can be compared to see if they have the same values, which they should if wave propagation was perfectly isotropic. As the figure shows, the 19-point face+edges stencil ($\nabla^2_{fe}$) produces nearly perfect isotropic wave propagation, with cells at the same distance in all directions having essentially the same values (max standard deviation = 0.000496, only 1% of maximum wave magnitude). In contrast, the standard 7-point faces-only case ($\nabla^2_f$) shows considerable levels of error, and a correspondingly rough mean value curve (max SD=.00742, nearly 17% of max wave magnitude). The 27-point stencil ($\nabla^2_{fec}$) exhibits an intermediate level of error (max SD=.00386, 8% of max wave magnitude, not shown). The improved symmetry of the 19-point case relative to the 27-point case is presumably because the 19-point case only includes a mutually orthogonal set of neighborhood points,

whereas the 27-point case includes additional non-orthogonal points.

## 7. Conclusion

The results presented herein demonstrate that including more neighbors in the computation of the Laplacian produces both faster and more rotationally symmetric results relative to the standard 7-point stencil. For maximum computational speed, the 27-point stencil is the best option, as it has the largest stable step size and the additional neighbors do not incur substantial increased cost on modern vectorizing processors. For maximum rotational symmetry, the 19-point stencil appears to be the best option. However, each of these large-stencil versions are both significantly faster and more rotationally symmetric than the standard 7-point stencil, which suggests that they should be widely adopted in numerical simulations involving the Laplacian operator.

## 8. Appendix: Discrete Gradients with Neighbor Averaging

The 27-point stencil can also be derived by way of a first-order gradient computation that uses more than the standard cartesian axis neighbors. The standard discrete gradient computation in one dimension involves averaging the two difference equations on either side of the point in question:

$$\begin{aligned} D^{-}\varphi_i &= \frac{1}{h}(\varphi_i - \varphi_{i-1}) \\ D^{+}\varphi_i &= \frac{1}{h}(\varphi_{i+1} - \varphi_i) \\ \frac{\partial \varphi}{\partial x} \approx \frac{1}{2}(D^{+}\varphi_i + D^{-}\varphi_i) &= \frac{1}{2h}(\varphi_{i+1} - \varphi_{i-1}) \end{aligned} \tag{34}$$

In three dimensions, the averaging process can be taken further by including rays through all neighboring points that have some projection along the gradient axis (Figure 4), with the contribution

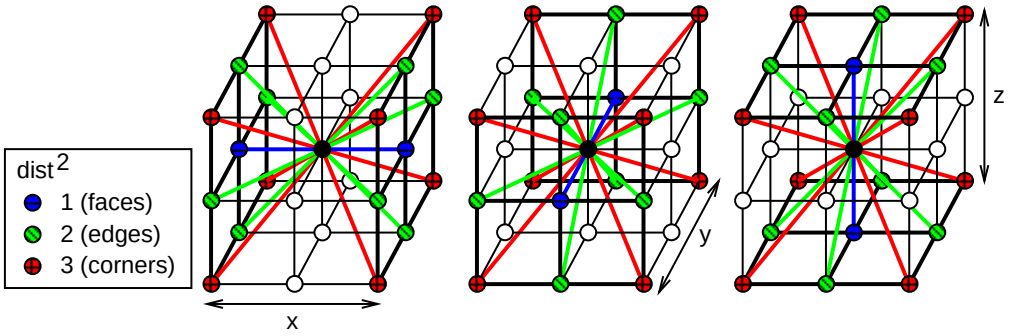


Figure 4. Computation of the first order spatial gradient using all 18 neighbors that have a non-zero projection along a given axis. Each neighbor contributes to the gradient in proportion with its projection along the axis (1 for face points, $\frac{1}{\sqrt{2}}$ for edges, and $\frac{1}{\sqrt{3}}$ for corners. Note that, across all three cases, the faces occur once, edges occur twice, and corners in all three cases (i.e., in proportion to their respective distances).

of each neighbor pair weighted by the extent of its projection along the axis:

$$\frac{\partial \varphi}{\partial x} \approx \frac{1}{h(2+\frac{8}{\sqrt{2}}+\frac{8}{\sqrt{3}})}\Big( \quad (\varphi_{(1,0,0)} - \varphi_{(-1,0,0)}) + \frac{1}{\sqrt{2}} \sum_{j \in \mathcal{N}_e} (\varphi_{j+} - \varphi_{j-}) + \frac{1}{\sqrt{3}} \sum_{j \in \mathcal{N}_c} (\varphi_{j+} - \varphi_{j-}) \Big) \tag{35}$$

where the neighborhoods $\mathcal{N}_e$ and $\mathcal{N}_c$ denote pairs of points $j+$ and $j-$ along the 4 rays through the edges and corners, respectively. The normalizing factor ensures that the weighted average sums to one.

Plugging this first-order gradient into the second-order difference-of-differences equation results in:

$$\frac{\partial^2 \varphi}{\partial x^2} \approx \frac{1}{h^2(1+\frac{4}{2}+\frac{4}{3})}\Big( \quad (\varphi_{(1,0,0)} + \varphi_{(-1,0,0)} - 2\varphi_i) + \frac{1}{2} \sum_{j \in \mathcal{N}_e} (\varphi_{j+} + \varphi_{j-} - 2\varphi_i) + \frac{1}{3} \sum_{j \in \mathcal{N}_c} (\varphi_{j+} + \varphi_{j-} - 2\varphi_i) \Big) \tag{36}$$

Which can be simplified by using sums over the individual neighbor points, instead of considering the rays:

$$\frac{\partial^2 \varphi}{\partial x^2} \approx \frac{3}{h^2 13} \left( \sum_{j \in \mathcal{N}_f} (\varphi_j - \varphi_i) + \frac{1}{2} \sum_{j \in \mathcal{N}_e} (\varphi_j - \varphi_i) + \frac{1}{3} \sum_{j \in \mathcal{N}_c} (\varphi_j - \varphi_i) \right) \tag{37}$$

We can then compute the Laplacian by summing together the derivatives along the three axes computed according to equation 37. However, the neighborhood of points involved for computing

the derivatives along each axis overlaps partially with the others, as shown in Figure 4. Interestingly, this overlap is different depending on the distance of the neighbor, in exact proportion to this distance: faces appear once, edges appear twice, and corners appear three times. Thus, if one were to combine all the terms in the sums into a single computation operating across all the neighbors, this differential repetition of neighbors would exactly cancel out the distance-based normalization factors ($\frac{1}{2}$, $\frac{1}{3}$). However, it does not make sense to overcount the influence of some neighbors versus others. Therefore, we can simply drop the repeated factors from the equation, which then includes all of the 26 neighbors exactly once, and one arrives at equation 22. It is interesting to note that both approaches arrive at the same $\frac{3}{13}$ normalization factor, via somewhat different routes.

## Acknowledgments

Thanks to Dwight Barkley and Toshinori Munakata for helpful comments.

## REFERENCES

1. M. Dowle, R. M. Mantel, and D. Barkley. Fast simulations of waves in three-dimensional excitable media. *International Journal of Bifurcation and Chaos* 1997; **7**:2529–2545.